

RESEARCH ARTICLE

Recycling augmented Lagrangian preconditioner in an incompressible fluid solver[†]

Maxim A. Olshanskii*¹ | Alexander Zhiliakov²

¹ Department of Mathematics, University of Houston, Houston, TX, USA

² Department of Mathematics, University of Houston, Houston, TX, USA

Correspondence

*Maxim A. Olshanskii, Department of Mathematics, University of Houston, Houston, TX 77204, USA. Email: maolshanskiy@uh.edu

Abstract

The paper discusses a reuse of matrix factorization as a building block in the Augmented Lagrangian (AL) and modified AL preconditioners for non-symmetric saddle point linear algebraic systems. The strategy is applied to solve two-dimensional incompressible fluid problems with efficiency rates independent of the Reynolds number. The solver is then tested to simulate motion of a surface fluid, an example of a 2D flow motivated by an interest in lateral fluidity of inextensible viscous membranes. Numerical examples include the Kelvin–Helmholtz instability problem posed on the sphere and on the torus. Some new eigenvalue estimates for the AL preconditioner are derived.

KEYWORDS:

Augmented Lagrangian preconditioner; grad-div stabilization; surface fluids; fluidic membranes; trace finite element method; Kelvin–Helmholtz instability

1 | INTRODUCTION

Augmented Lagrangian (AL) preconditioning is a potent technique that has been developed to solve some highly non-symmetric algebraic systems having a saddle point structure^{1–11}. The need to treat such problems numerically emerges from the discretization of systems of PDEs describing the motion of incompressible viscous fluid with dominating inertia effects. Adopting the terminology of fluid mechanics, the AL approach augments the velocity subproblem of the system using a suitably weighted incompressibility constraint. This leads to a well conditioned pressure Schur complement matrix, but makes the velocity submatrix more difficult to solve or to precondition. Already in the original work¹ a special multigrid method has been used to overcome the difficulty associated with preconditioning the velocity block, and recently this technique was extended in^{12, 13}. Nevertheless, the specialized multilevel approach is efficient only if a hierarchy of nested discretizations is available and only for certain finite element velocity–pressure pairs. In the present paper we advocate a more general but still efficient, way to handle the velocity subproblem in the AL approach. The proposed method consists of computing a (possibly incomplete) LU factorization of the velocity block (or velocity sub-blocks in a modified AL approach) with further recycling of the factors over several time steps. The factorization can be updated when the velocity field variations significantly change the transport term in the equations. A simpler strategy adopted here consists of updating preconditioner when the number of FGMRES iterations exceeds a threshold. We shall see that for realistic unsteady 2D flows this results in a very efficient approach, which is robust with respect to the Reynolds number and calls for only a small number of full factorizations over a long-time simulation.

Employing matrix factorizations in algebraic solvers for equations governing the flow of viscous incompressible fluids is not a new theme. It is standard to factorize the discrete pressure Poisson equation. More recently, studies were done regarding different strategies to perform incomplete LU factorization of the coupled systems for velocity and pressure^{14–17}. We note that

[†]This work was partially supported by US National Science Foundation (NSF) through grants DMS-1953535 and DMS-2011444.

the latter cannot be done with the help of position-based ILU, since the pressure block in the matrix may be zero. The augmented Lagrangian approach provides a framework to apply factorization only to the velocity matrix, while retaining the overall excellent preconditioning properties. The velocity matrix results from the discretization of an elliptic part of the system. Therefore it is typically a positive definite matrix and LU factorization is stable without any preprocessing.

Large scale 3D simulations lead to algebraic systems which are still too expensive to factorize exactly and alternative ways of treating the velocity submatrix, e.g. based on geometric/algebraic multigrid, domain decomposition methods or incomplete factorization, can be more feasible and practical. The situation is different for 2D problems, where acceptable resolution is often achieved using the number of degrees of freedom affordable by state-of-the-art direct solvers executed on a desktop machine. Traditionally 2D flows have been considered as a mathematical idealization of real-life 3D phenomena. However, recently we see a growing interest in understanding and solving fluid systems posed on 2D surfaces (see, e.g.,^{18–30}) as physically motivated continuum based models of thin material layers exhibiting lateral viscosity such as lipid bilayers and plasma membranes^{31–33}.

This recent interest in models describing lateral fluidity of material surfaces motivates our choice of the test fluid problem here. We consider the Navier–Stokes equations posed on a geometrically steady surface. These equations govern the tangential viscous motions of the surface fluid subject to the inextensibility condition. A geometrically unfitted discretization technique known as the trace finite element method (Trace FEM)^{34,35} is applied to handle the systems numerically. The augmentation is added on finite element (FE) level in the form of the grad-div stabilization^{36,37}. For such a setting, we prove eigenvalue bounds for the preconditioned system that extend a result from¹ for the case of the unfitted surface FEM and the FE-level augmentation. Compared to the case treated in¹ and other publications, the FE-level augmentation delivers a different algebraic structure. The latter required us to search for different arguments to prove the eigenvalue bounds. A preconditioned iterative method with recycled factorizations is then applied to solve the linearized Navier–Stokes equations on each time step of numerical simulations. The whole approach is used to compute two interesting surface flows: the Kelvin–Helmholtz instability problem on a sphere and a torus. We observe a notable difference in the evolution of (large) vortices in these two settings.

Summarizing, the paper contributes to the field of developing fast and reliable solvers for fluid problems by (i) Introducing a simple and efficient strategy to reuse factorizations of positive definite matrices leading to a solver robust with respect to the Reynolds number; (ii) Extending the AL preconditioner and its eigenvalue analysis to the trace FEM discretization of the linearized surface Navier–Stokes equations. Our construction can be useful for other unfitted FEMs for fluid equations. Equipped with these tools we simulate for the first time the Kelvin–Helmholtz instability on a torus.

The remainder of the paper consists of three sections. In section 2 we recall the surface Navier–Stokes equations and apply \mathbf{P}_2 – P_1 Trace FEM to discretize them. Section 3 considers the properties of the resulting linear algebraic systems, introduces a preconditioner, eigenvalue bounds, and recycling strategy. A proof of the bounds is given in the Appendix section. Finally, section 4 collects and discusses the results of numerical experiments.

2 | SURFACE NAVIER–STOKES PROBLEM AND ITS DISCRETIZATION

Consider a closed sufficiently smooth surface Γ embedded in \mathbb{R}^3 . For \mathbf{n} , the outward pointing unit normal on Γ , the orthogonal projection on the tangential plane is given by $\mathbf{P} = \mathbf{P}(\mathbf{x}) := \mathbf{I} - \mathbf{n}(\mathbf{x})\mathbf{n}(\mathbf{x})^T$, $\mathbf{x} \in \Gamma$. Following²² we formulate the surface fluid equation in terms of tangential differential calculus. To this end, we assume smooth extensions of a scalar function $p : \Gamma \rightarrow \mathbb{R}$ or a vector function $\mathbf{u} : \Gamma \rightarrow \mathbb{R}^3$ to a neighborhood $\mathcal{O}(\Gamma)$ of Γ . For example, one can consider extension along the normal directions using the closest point mapping $\mathbf{p} : \mathcal{O}(\Gamma) \rightarrow \Gamma$. The surface gradient and covariant derivatives on Γ are then defined as $\nabla_\Gamma p = \mathbf{P}\nabla p^e$ and $\nabla_\Gamma \mathbf{u} := \mathbf{P}\nabla \mathbf{u}^e \mathbf{P}$. The definitions of surface gradient and covariant derivatives are independent of a particular smooth extension of p and \mathbf{u} off Γ . The surface rate-of-strain tensor³¹ is given by $E_s(\mathbf{u}) := \frac{1}{2}(\nabla_\Gamma \mathbf{u} + \nabla_\Gamma \mathbf{u}^T)$, and the surface divergence operators for a vector $\mathbf{u} : \Gamma \rightarrow \mathbb{R}^3$ and a tensor $\mathbf{A} : \Gamma \rightarrow \mathbb{R}^{3 \times 3}$ are defined as

$$\operatorname{div}_\Gamma \mathbf{u} := \operatorname{tr}(\nabla_\Gamma \mathbf{u}), \quad \operatorname{div}_\Gamma \mathbf{A} := \left(\operatorname{div}_\Gamma(\mathbf{e}_1^T \mathbf{A}), \operatorname{div}_\Gamma(\mathbf{e}_2^T \mathbf{A}), \operatorname{div}_\Gamma(\mathbf{e}_3^T \mathbf{A}) \right)^T,$$

with \mathbf{e}_i the i th basis vector in \mathbb{R}^3 .

The conservation of momentum for a thin material layer together with the inextensibility condition and assumption of vanishing normal motions (geometric equilibrium) leads to the following surface Navier–Stokes problem: Given area forces $\mathbf{f} \in L^2(\Gamma)^3$,

with $\mathbf{f} \cdot \mathbf{n} = 0$, find a vector field $\mathbf{u} : [0, T] \times \Gamma \rightarrow \mathbb{R}^3$, with $\mathbf{u}(0, \cdot) = \mathbf{u}_0$, $\mathbf{u} \cdot \mathbf{n} = 0$, and $p : [0, T] \times \Gamma \rightarrow \mathbb{R}$ such that

$$\begin{cases} \rho \left(\frac{\partial \mathbf{u}}{\partial t} + (\nabla_{\Gamma} \mathbf{u}) \mathbf{u} \right) - 2\nu \mathbf{P} \operatorname{div}_{\Gamma}(E_s(\mathbf{u})) + \nabla_{\Gamma} p = \mathbf{f} & \text{on } \Gamma, \\ \operatorname{div}_{\Gamma} \mathbf{u} = 0 & \text{on } \Gamma. \end{cases} \quad (1)$$

Here \mathbf{u} is the tangential fluid velocity, p is the surface fluid pressure, ρ and ν are density and viscosity coefficients. We further assume ν , p and \mathbf{f} are re-scaled so that $\rho = 1$.

For time discretization, we assume a constant time step $\Delta t = T/N$ and adopt the notation $\mathbf{u}^k(\mathbf{x})$ for velocity solution at time $t^k = k\Delta t$, and similar for p^k . A semi-implicit time-stepping scheme for (1) reads: Given \mathbf{u}^{k-1} , \mathbf{u}^{k-2} , find \mathbf{u}^k s.t. $\mathbf{u}^k \cdot \mathbf{n} = 0$ and p^k solving

$$\begin{cases} [\mathbf{u}]_t^k + (\nabla_{\Gamma} \mathbf{u}^k) \tilde{\mathbf{u}}^k - 2\nu \mathbf{P} \operatorname{div}_{\Gamma}(E_s(\mathbf{u}^k)) + \nabla_{\Gamma} p^k = \mathbf{f}^k & \text{on } \Gamma, \\ \operatorname{div}_{\Gamma} \mathbf{u}^k = 0 & \text{on } \Gamma \end{cases} \quad (2)$$

for $k = 2, 3, \dots, N$. In numerical experiments we employ the second order method with

$$[\mathbf{u}]_t^k = \frac{3\mathbf{u}^k - 4\mathbf{u}^{k-1} + \mathbf{u}^{k-2}}{2\Delta t}, \quad \tilde{\mathbf{u}}^k = 2\mathbf{u}^{k-1} - \mathbf{u}^{k-2}, \quad (3)$$

but this particular choice has little effect on the properties of the resulting linear systems.

We see that on each time step the linearized problem in (2) is the Oseen-type system

$$\begin{aligned} \alpha \mathbf{u} + (\nabla_{\Gamma} \mathbf{u}) \mathbf{w} - 2\nu \mathbf{P} \operatorname{div}_{\Gamma}(E_s(\mathbf{u})) + \nabla_{\Gamma} p &= \mathbf{f}, \\ \operatorname{div}_{\Gamma} \mathbf{u} &= 0 \end{aligned} \quad (4)$$

with $\alpha \simeq \Delta t^{-1}$, the wind field $\mathbf{w} := \tilde{\mathbf{u}}^k$, and \mathbf{f} collects contributions from the area forces and from the previous step velocities of the discretized time derivative. Hence the resulting system of linear algebraic equations is non-symmetric and of saddle-point type with properties resembling those of the planar Oseen system, well-studied problem; see, e.g.^{38,39}. In particular, the problem is increasingly hard to solve when ν goes to zero. One way to avoid this increasing complexity of the linear algebra system is to lag the entire inertia term in time, e.g. to replace the second term in (2) with $(\nabla_{\Gamma} \tilde{\mathbf{u}}^k) \tilde{\mathbf{u}}^k$, ending up with a symmetric Stokes-type problem, same on each time step. However, numerical stability of such implicit-explicit scheme is known⁴⁰ to impose a time step restriction of the form $\Delta t \leq c(\nu)h^d$, where $d = 2$ for two-dimension flows and $c(\nu)$ decreasing for $\nu \rightarrow 0$. This leads to a serious growth of computational costs for small h and ν despite the ease of linear algebra. In contrast, (2) is unconditionally stable⁴¹ (approximation analysis suggest $\Delta t \approx h$), and our strategy here is to alleviate computational costs by employing a more sophisticated linear algebra solve re-enforced by the recycling algorithm.

A weak formulation of (4) requires the closed subspace of $H^1(\Gamma)^3$ consisting of *tangential* vector fields, $\mathbf{V}_T := \{\mathbf{v} \in H^1(\Gamma)^3 \mid \mathbf{v} \cdot \mathbf{n} = 0\}$. \mathbf{V}_T serves as the velocity trial and test space in a weak formulation. If desired, the tangentiality constraint can be relaxed in a penalty weak formulation²² that allows for the larger velocity space: $\{\mathbf{v} \in L^2(\Gamma)^3 : \mathbf{P}\mathbf{v} \in \mathbf{V}_T\}$. The well-posedness of both formulations relies on the surface Korn inequality (see (4.8) in²²): There exists a constant $c_K > 0$ such that

$$\|\mathbf{u}\|_{L^2(\Gamma)} + \|E_s(\mathbf{u})\|_{L^2(\Gamma)} \geq c_K \|\mathbf{u}\|_{H^1(\Gamma)} \quad \text{for all } \mathbf{u} \in \mathbf{V}_T, \quad (5)$$

and the inf-sup condition (Lemma 4.2 in²²): There exists a constant $c_0 > 0$ such that the following holds:

$$\inf_{p \in L^2_0(\Gamma)} \sup_{\mathbf{v} \in \mathbf{V}_T} \frac{\int_{\Gamma} q \operatorname{div}_{\Gamma} \mathbf{u} \, ds}{\|\mathbf{v}\|_{H^1(\Gamma)} \|p\|_{L^2(\Gamma)}} \geq c_0. \quad (6)$$

For the discretization of (4) we apply the trace \mathbf{P}_2 - P_1 FEM²⁸. To apply the method, assume Γ is strictly contained in a polygonal domain $\Omega \subset \mathbb{R}^3$ and consider a family $\{\mathcal{T}_h\}_{h>0}$ of shape regular tetrahedral tessellations of Ω . Tetrahedra that have a nonzero intersection with Γ are collected in the set denoted by \mathcal{T}_h^{Γ} with the characteristic mesh size h , and $\overline{\Omega}_h^{\Gamma} = \bigcup \{\overline{T} : T \in \mathcal{T}_h^{\Gamma}\}$. On $\overline{\Omega}_h^{\Gamma}$ we consider the standard H^1 -conforming finite element spaces of degree k ,

$$V_h^k = \{v \in C(\overline{\Omega}_h^{\Gamma}) : v \in P_k(T) \text{ for any } T \in \mathcal{T}_h^{\Gamma}\}, \quad \text{with } k = 1, 2.$$

The velocity and pressure bulk finite element spaces are then defined to be

$$\mathbf{V}_h := (V_h^2)^3, \quad Q_h := V_h^1 \cap L^2_0(\Gamma).$$

The finite element formulation uses the restrictions (traces) of these spaces on Γ . Note that traces of vector functions from \mathbf{V}_h does not necessarily satisfy the tangentiality $\mathbf{u} \cdot \mathbf{n} = 0$ condition. It is not straightforward, if possible at all, to build an H^1 -conforming

finite element method which is also conformal with respect to the tangentiality condition. Therefore, the tangentiality condition will be enforced weakly by the penalty method. We shall also need an extension of the normal vector from Γ to Ω_h^Γ , which we define as $\mathbf{n} = \nabla d$, where d is the signed distance function to Γ . In practice, d is often not available and an approximation is used. We introduce the following finite element bilinear forms:

$$\begin{aligned} a(\mathbf{u}, \mathbf{v}) &:= \int_{\Gamma} (\alpha \mathbf{u} \cdot \mathbf{v} + \mathbf{v}^T (\nabla_{\Gamma} \mathbf{u}) \mathbf{w}) ds + 2\nu \int_{\Gamma} E_s(\mathbf{u}) : E_s(\mathbf{v}) ds \\ &\quad + \tau \int_{\Gamma} (\mathbf{n} \cdot \mathbf{u})(\mathbf{n} \cdot \mathbf{v}) ds + \rho_u \int_{\Omega_h^\Gamma} [(\mathbf{n} \cdot \nabla) \mathbf{u}] \cdot [(\mathbf{n} \cdot \nabla) \mathbf{v}] dx, \\ b(\mathbf{v}, q) &:= - \int_{\Gamma} q \operatorname{div}_{\Gamma} \mathbf{v} ds = \int_{\Gamma} \nabla_{\Gamma} q \cdot \mathbf{v} ds, \\ \gamma(\mathbf{u}, \mathbf{v}) &:= \hat{\gamma} \int_{\Gamma} \operatorname{div}_{\Gamma} \mathbf{u} \operatorname{div}_{\Gamma} \mathbf{v} ds, \quad s(p, q) := \rho_p \int_{\Omega_h^\Gamma} (\mathbf{n} \cdot \nabla p)(\mathbf{n} \cdot \nabla q) dx. \end{aligned}$$

The forms are well defined for $p, q \in H^1(\Omega_h^\Gamma)$, $\mathbf{u}, \mathbf{v} \in H^1(\Omega_h^\Gamma)^3$. The finite element formulation of (4) then reads: Find $\{\mathbf{u}_h, p_h\} \in \mathbf{V}_h \times Q_h$ solving

$$\begin{aligned} a(\mathbf{u}_h, \mathbf{v}_h) + \gamma(\mathbf{u}_h, \mathbf{v}_h) + b(\mathbf{v}_h, p_h) &= (\mathbf{f}, \mathbf{v}_h), \\ b(\mathbf{u}_h, q_h) - s(p_h, q_h) &= 0 \end{aligned} \quad (7)$$

for all $\mathbf{v}_h \in \mathbf{V}_h$ and $q_h \in Q_h$. In the definition of the forms, $\tau > 0$ is a penalty parameter and $\rho_u \geq 0$, $\rho_p \geq 0$ are stabilization parameters, which we set according to²⁸:

$$\tau = h^{-2}, \quad \rho_p = h, \quad \rho_u = 1. \quad (8)$$

Note that both stabilization terms vanish if \mathbf{u} and p is the surface solution extended along normal directions to a neighborhood of Γ . This makes the finite element formulation consistent. At the same time, both terms add to the finite element formulation additional ‘‘stiffness’’ in the normal direction. This allows to eliminate the dependence of the resulting algebraic systems condition number on the position of Γ in the background mesh, the idea first suggested for trace FEM in⁴² and later explored in many publications on unfitted FEM for surface PDEs, e.g.^{43–45} (the particular choice of stabilization terms varies in the literature). We refer to²⁸ for the further discussion of the role of these terms in the context of unfitted \mathbf{P}_2 – P_1 elements, the proof of the well-posedness of the finite element formulation, error analysis, and the proof of Γ -independent estimates on the condition numbers of the velocity and pressure matrices.

The fourth term in (7) is the surface analogue of the grad-div stabilization^{36, 37}. We further set $\hat{\gamma} = 1$ unless it is stated otherwise and write $\gamma = \hat{\gamma}$ to simplify the notation. We do not study the dependence of optimal γ on other parameters of the finite element formulation. It is known⁴⁶ that there is a wide range of quasi-optimal γ -s, where the solution quality is almost insensitive to the variation of the parameter. Hence γ can be taken smaller or larger depending on other considerations. For simplicity we adopt $\gamma = 1$ for the full AL approach and mesh-dependent γ for the modified AL approach; see the next section. It is interesting that no other stabilization was found to be necessary for computations with high Reynolds numbers. A possible explanation is that tangential flows do not produce boundary layers (on a closed surface) and, in addition, the grad-div term by itself is known to dissipate excessive energy in under-resolved simulation^{46, 47}.

We conclude this section noting that the implementation requires the integration of polynomial functions over Γ . In practice this is avoided by approximating Γ by some Γ_h which admits exact quadrature rules. The quantification of the introduced geometric inconsistency in the case of the Stokes problem and \mathbf{P}_k – P_{k-1} , $k = 2, 3, \dots$, trace elements is given in⁴⁸.

3 | SYSTEM OF LINEAR ALGEBRAIC EQUATIONS AND PRECONDITIONING

We now turn to the matrix form of the discretized surface Oseen system and define the velocity, pressure stabilization and divergence constraint matrices:

$$\mathbf{A}_{i,j} = a(\psi_j, \psi_i) + \gamma(\psi_j, \psi_i), \quad \mathbf{C}_{k,m} = s(\xi_k, \xi_m), \quad \mathbf{B}_{k,i} = b(\psi_i, \xi_k),$$

where $\{\psi_j\}$ and $\{\xi_k\}$ are the velocity and pressure nodal basis functions spanning \mathbf{V}_h and \mathbf{Q}_h , respectively. After arranging velocity degrees of freedom first and pressure degrees of freedom next, we arrive at the system with the 2×2 -block matrix:

$$\underbrace{\begin{bmatrix} \mathbf{A} & \mathbf{B}^T \\ \mathbf{B} & -\mathbf{C} \end{bmatrix}}_{\mathcal{A}} \begin{bmatrix} \mathbf{u} \\ p \end{bmatrix} = \begin{bmatrix} \mathbf{f} \\ 0 \end{bmatrix}. \quad (9)$$

An important matrix related to the above system is the pressure Schur complement $\mathbf{S} = \mathbf{B}\mathbf{A}^{-1}\mathbf{B}^T + \mathbf{C}$, which results after elimination of the velocity unknowns from the system. A preconditioner for \mathbf{S} is a necessary ingredient for most iterative solvers that exploit the block structure of \mathcal{A} . Following a common practice³⁹ we consider the block-triangle right preconditioner for \mathcal{A} :

$$\mathcal{P} := \begin{pmatrix} \hat{\mathbf{A}} & \mathbf{B}^T \\ & \hat{\mathbf{S}} \end{pmatrix}, \quad (10)$$

where $\hat{\mathbf{A}}$ and $\hat{\mathbf{S}}$ are preconditioners for \mathbf{A} and \mathbf{S} , respectively.

For the next step, we define the surface pressure mass matrix \mathbf{M}_p and the pressure Laplace–Beltrami matrix \mathbf{L}_p :

$$(\mathbf{M}_p)_{k,m} = \int_{\Gamma} \xi_k \xi_m ds, \quad (\mathbf{L}_p)_{k,m} = \int_{\Gamma} \nabla_{\Gamma} \xi_k \cdot \nabla_{\Gamma} \xi_m ds.$$

For the surface Stokes problem ($\alpha = 0$, $\mathbf{w} = 0$, $\gamma = 0$, $\nu = 1$) matrix \mathbf{S} is spectrally equivalent to the stabilized pressure mass matrix $\mathbf{M}_p + \mathbf{C}$; see²⁸. However, for $\mathbf{w} \neq 0$, $\gamma = 0$, and $\nu \rightarrow 0$ the problem of building a suitable preconditioner for \mathbf{S} is known to be particular difficult. To circumvent it, the authors of¹ introduced an augmentation to the \mathbf{A} block of the system replacing \mathbf{A} with $\mathbf{A} + \gamma \mathbf{B}^T \mathbf{M}_p^{-1} \mathbf{B}$. Such augmentation is not algebraically consistent in our case, since $\mathbf{C} \neq 0$ and so $\mathbf{B}\mathbf{u} \neq 0$. We note that $\mathbf{C} \neq 0$ is a typical situation for many unfitted *inf-sup stable* FEM discretizations of the (Navier–)Stokes equations (both in volumes and on surfaces) as well as for stabilized elements⁴⁹. Hence, we suggest to introduce the augmentation on the finite element level, i.e. to add the grad-div term.

For the planar Oseen problem discretized with standard \mathbf{P}_2 – \mathbf{P}_1 elements one can show that the Schur complement of the algebraically augmented matrix is spectrally equivalent to the pressure mass matrix scaled by $(\gamma + \nu)^{-1}$ for sufficiently large γ . We show here that similar property holds for the trace FEM and when the algebraic augmentation is replaced by the grad-div stabilization and so the augmentation term is not of the $\gamma \mathbf{B}^T \mathbf{M}_p^{-1} \mathbf{B}$ form. More precisely, assume $\alpha = 0$, $\nu \leq 1$, $\|\mathbf{w}\|_{L^\infty(\Gamma)} = 1$ and the skew-symmetric discretization of the advection term (A2) (these assumptions are standard for the analysis, but can be relaxed for the expense of extra technical details), then the eigenvalues of

$$\mathbf{S}p = \lambda((\nu + \gamma)^{-1} \mathbf{M}_p + \mathbf{C})p \quad (11)$$

satisfy the following bound

$$c \frac{\gamma + \nu}{\gamma + \nu^{-1}} \leq \Re(\lambda), \quad |\lambda| \leq \frac{\nu + \gamma}{\gamma}, \quad (12)$$

with some positive c independent of problem parameters and the position of Γ in the background mesh. $\Re(\lambda)$ above denotes the real part of λ . We include the proof in the Appendix. We see that for large enough γ all eigenvalues are contained in a box in the right half-plane with the bounds independent of ν . Motivated by (12) we define the Schur complement preconditioner through its inverse as follows:

$$\hat{\mathbf{S}}^{-1} := ((\nu + \gamma)^{-1} \mathbf{M}_p + \mathbf{C})^{-1} + (\alpha^{-1} \mathbf{L}_p + \mathbf{C})^{-1} \quad (13)$$

The second term is included to deal with the dominating reaction term in the Oseen problem (4) if $\alpha \gg 1$. This part of $\hat{\mathbf{S}}^{-1}$ resembles the Cahouet–Chabard preconditioner⁵⁰. We apply several CG iterations to compute the action of $(\alpha^{-1} \mathbf{L}_p + \mathbf{C})^{-1}$ and $((\nu + \gamma)^{-1} \mathbf{M}_p + \mathbf{C})^{-1}$ on a vector. Alternatively, these matrices can be also one time factorized. Since the number of pressure degrees of freedom is much smaller than velocity ones, either choice marginally affects the total timings. Note also that $\alpha^{-1} \mathbf{L}_p + \mathbf{C}$ has a one-dimensional kernel, i.e. the subspace of constant pressures, which we easily handle by iterating in a proper subspace. Strictly speaking $(\alpha^{-1} \mathbf{L}_p + \mathbf{C})^{-1}$ is the pseudo-inverse in our case.

The augmentation has the downside of adding to the (1, 1)-block the term with a large nullspace. For larger γ this makes the matrix \mathbf{A} poor conditioned and hinders the efficiency of standard iterative methods to evaluate \mathbf{A}^{-1} . As a more flexible alternative we explore here direct LU factorization of \mathbf{A} (or its sub-blocks) and the reuse of the factors for several time steps. In pursuing this line, we consider two strategies of building $\hat{\mathbf{A}}$:

1. LU factorization of the full velocity block \mathbf{A} (full AL approach);

2. Velocity unknowns are enumerated componentwise so that \mathbf{A} attains the 3×3 -block form. $\hat{\mathbf{A}}$ is obtained from \mathbf{A}_{lr} , the block upper-triangle part of \mathbf{A} , by applying LU factorization to each individual diagonal block of \mathbf{A}_{lr} . This corresponds to modified AL approach from².

The modified AL approach allows to factorize smaller and better structured matrices that have the structure of a stiffness matrix of a conforming FEM applied to an elliptic scalar PDE. This enhanced efficiency comes with a price of slight ν and h dependence of the preconditioner performance². We shall see below that in the case of time-dependent 2D flow the price is very tolerable.

Same approaches, of course, apply to reusing ILU factorizations, but we fix our idea and consider below exact LU. The surface fluid problem is essentially 2D and the number of velocity unknowns allows applying LU factorization. Furthermore, in a curvilinear metric the viscosity term does not simplify to Laplace operators for each velocity component, i.e. for tangential divergence free \mathbf{u} we note that in general $\mathbf{P} \operatorname{div}_{\Gamma}(E_s(\mathbf{u})) \neq \Delta_{\Gamma} \mathbf{u}$ with a componentwise Laplace–Beltrami operator Δ_{Γ} . Therefore, \mathbf{A} does not have a block-diagonal structure for $\gamma = 0$ and so adding the γ -term does not change the sparsity pattern of the matrix (in contrast to the augmentation in the planar case).

To make the algorithm precise, denote by $\mathbf{L}(k)$ and $\mathbf{U}(k)$ the LU factors of $\mathbf{A}(k)$ at step k of (2). We let $\hat{\mathbf{A}} = \mathbf{L}(k)\mathbf{U}(k)$ to be the preconditioner for all $\mathbf{A}(k+m)$, $m = 0, \dots, M$, where $M \geq 0$ is the largest index such that

$$\frac{\#\operatorname{Iter}_{\text{FGMRES}}(k+m)}{\#\operatorname{Iter}_{\text{FGMRES}}(k)} \leq \kappa, \quad \text{for } m = 0, \dots, M, \quad (14)$$

where $\kappa \geq 1$ is a maximum allowed increase of the preconditioned FGMRES iterations without updating the preconditioner.

4 | NUMERICAL SIMULATIONS

We apply the trace FEM as described in section 2 to simulate the mixing layer of isothermal incompressible viscous surface fluid at several Reynolds numbers. The setup resembles the classical problem of the Kelvin–Helmholtz instability: For a detailed discussion of the planar analogue we refer to⁵¹ and references therein. At higher Reynolds numbers the flow exhibits sharp internal layers and intensive vortical dynamics, offering a good test problem for both discretizations and flow solvers.

For discretization, an initial triangulation \mathcal{T}_{h_0} was build by dividing $\Omega = (-\frac{5}{3}, \frac{5}{3})^3$ into 2^3 cubes and further splitting each cube into 6 tetrahedra with $h_0 = \frac{5}{3}$. Further, the mesh is refined only close to the surface, and $\ell \in \mathbb{N}$ denotes the level of refinement so that $h_{\ell} = \frac{5}{3} 2^{-\ell}$. The trace \mathbf{P}_2 – \mathbf{P}_1 Taylor–Hood finite element method with BDF2 time stepping is applied as described in (2)–(3), with the choice of parameters in (8). The choice of γ is $\gamma = 1$ in the full AL and a mesh-dependent γ in the modified AL. No further stabilizing terms, e.g., of streamline diffusion type, were included in the method, since the computed solutions do not reveal any spurious modes. We would like the discretization error, which results from the approximation of Γ , to be consistent with the higher order interpolation properties of \mathbf{P}_2 elements⁴⁸. To address this, we apply additional refinement to define a piecewise-linear surface Γ_h used for the purpose of numerical integration as described in^{28, section 6.3}. Software packages DROPS⁵² and Belos, Amesos from Trilinos⁵³ were used for matrices assembling and algebraic solver execution, respectively. Because of the additional refinement used to define numerical quadratures, the matrix assembling time grows superlinear in our examples. The optimal complexity here can be obtained by using isoparametric higher order trace elements⁵⁴, not however implemented in the software we use.

4.1 | The Kelvin–Helmholtz instability problem setup

There are very limited numerical studies of the Kelvin–Helmholtz (KH) problem for surface fluids. Examples of an isothermal KH flows on cylinder and on the unit sphere are given in^{24, 48}. Here we use the sphere example and for the first time simulate the KH flow on a torus of revolution.

The design of numerical experiment for the sphere follows^{24, 48}. For $\Gamma = \mathcal{S}^2$, let ξ and ζ to be renormalized azimuthal and polar coordinates, respectively: $-1/2 \leq \xi, \zeta < 1/2$. The tangent basis direction are $\mathbf{e}_{\xi} := \nabla_{\Gamma} \xi / \|\nabla_{\Gamma} \xi\|$ and $\mathbf{e}_{\zeta} := \nabla_{\Gamma} \zeta / \|\nabla_{\Gamma} \zeta\|$. The initial velocity field is given by the counter-rotating upper and lower hemispheres with velocity speed approximately equal 1 closer to equator and vanishing at poles. The velocity field has a sharp transition layer along equator, where we add perturbation

to trigger the development of the vortical strip:

$$\begin{aligned}\mathbf{u}_0(\xi, \zeta) &:= d(\zeta)(\tanh(2\zeta/\delta_0)\mathbf{e}_\xi + c_n \mathbf{curl}_\Gamma \psi), \\ \psi(\xi, \zeta) &:= e^{-(\zeta/\delta_0)^2} (a_a \cos(m_a \pi \xi) + a_b \cos(m_b \pi \zeta)),\end{aligned}\tag{15}$$

where d is the distance from Γ to the z -axis. We take $\delta_0 := 0.05$ (for $|z| \gtrsim \delta_0$ the velocity field is close to a rigid body rotation around the z -axis), $c_n := 10^{-2}$ (perturbation parameter), and $a_a = 1$, $m_a = 16$, $a_b = 0.1$, $m_b = 20$ (perturbation magnitudes and frequencies). Note that \mathbf{u}_0 is tangential by construction. The Reynolds number $Re \simeq v^{-1}\delta_0$ is based on $\|\mathbf{u}\|_{L^\infty(\Gamma)} \simeq 1$ and the initial layer width. We ran numerical simulations with $v = \frac{1}{2}10^{-k}$, for $k = 3, 4, 5$, which corresponds to $Re = 10^k$, $k = 2, 3, 4$.

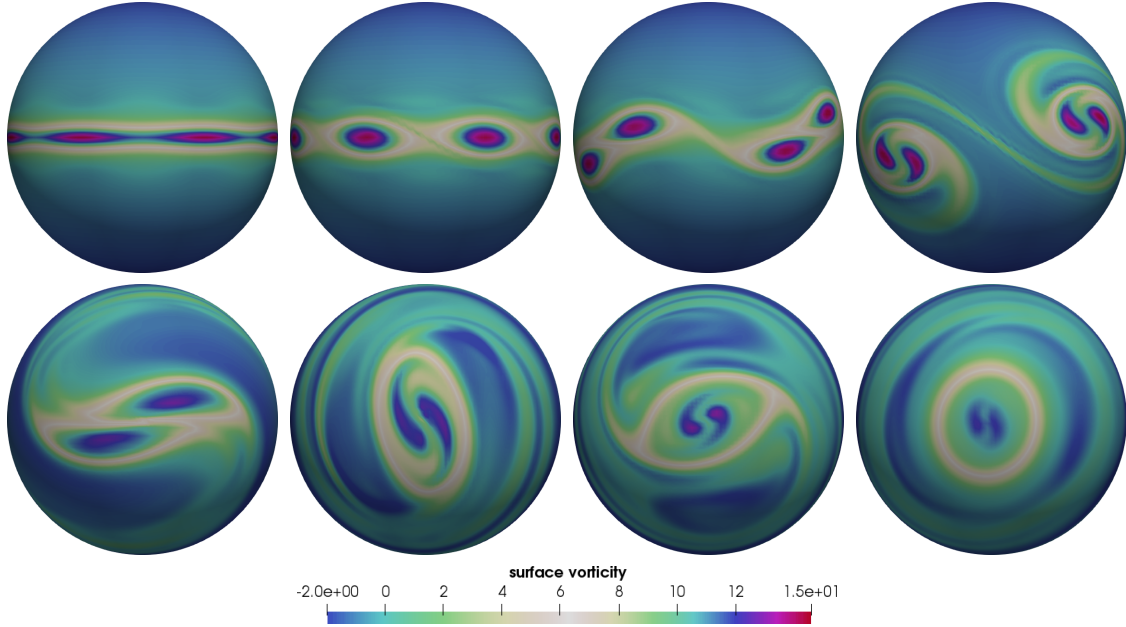


FIGURE 1 KH flow at $Re = 10^4$. Snapshots of surface vorticity $w_h = \mathbf{curl}_{\Gamma_h} \mathbf{u}_h$ for $t \in \{0, 2.5, 5, 6.25, 10, 12.5, 15, 20\}$. [Click here](#) for the full animation.

In Figure 1 we show several snapshots of the surface vorticity distributions starting from the initial condition. The solution reproduces the well known flow pattern of the planar KH instability development, which includes the initial vortices formation in the layer followed by pairing and self-organization into larger vortices. At the final simulation time we see two large counter-rotating vortices. The dissipation rate for this solution was studied in⁴⁸ confirming the qualitatively correct behaviour.

The second example we consider is KH instability on two-dimensional torus $\Gamma = \mathbb{T}^2 = \{\mathbf{x} \in \Omega \mid r^2 = x_3^2 + (\sqrt{x_1^2 + x_2^2} - R)^2\}$, with $R = 1$ and $r = 0.5$. The coordinate system is (ρ, ϕ, θ) , with

$$\mathbf{x} = R \begin{pmatrix} \cos \phi \\ \sin \phi \\ 0 \end{pmatrix} + \rho \begin{pmatrix} \cos \phi \cos \theta \\ \sin \phi \cos \theta \\ \sin \theta \end{pmatrix},$$

where ρ -direction is normal to Γ , $\frac{\partial \mathbf{x}}{\partial \rho} \perp \Gamma$ for $\mathbf{x} \in \Gamma$. In the torus coordinates, the initial velocity field is given by the same formula (15) with $\xi = \psi/(2\pi)$, $\zeta = \theta/(2\pi)$, and $d(\zeta) := d(\mathbf{x}(\xi, \zeta)) = \sqrt{x^2 + y^2} - 0.5$, $\mathbf{x} = (x, y, z)$, so that $d(\zeta)$ vanishes on the inner ring of the torus.

Figure 2 visualizes the vorticity field of the KH flow on the torus for $Re = 10^4$ ($v = \frac{1}{2}10^{-5}$). The initial stage of the vortical layer formation and small vortices pairing is similar to the case of the sphere and the plane. The different geometry (and topology) of the torus apparently affects the interaction of larger vortices. From the time of about 20 units there are 4 large vortices formed, which further travel in the both toroidal and poloidal directions without pairing up to time $t = 45$, after $t = 45$ the motions loses any apparent axial symmetry and becomes rather complex (see the animation).

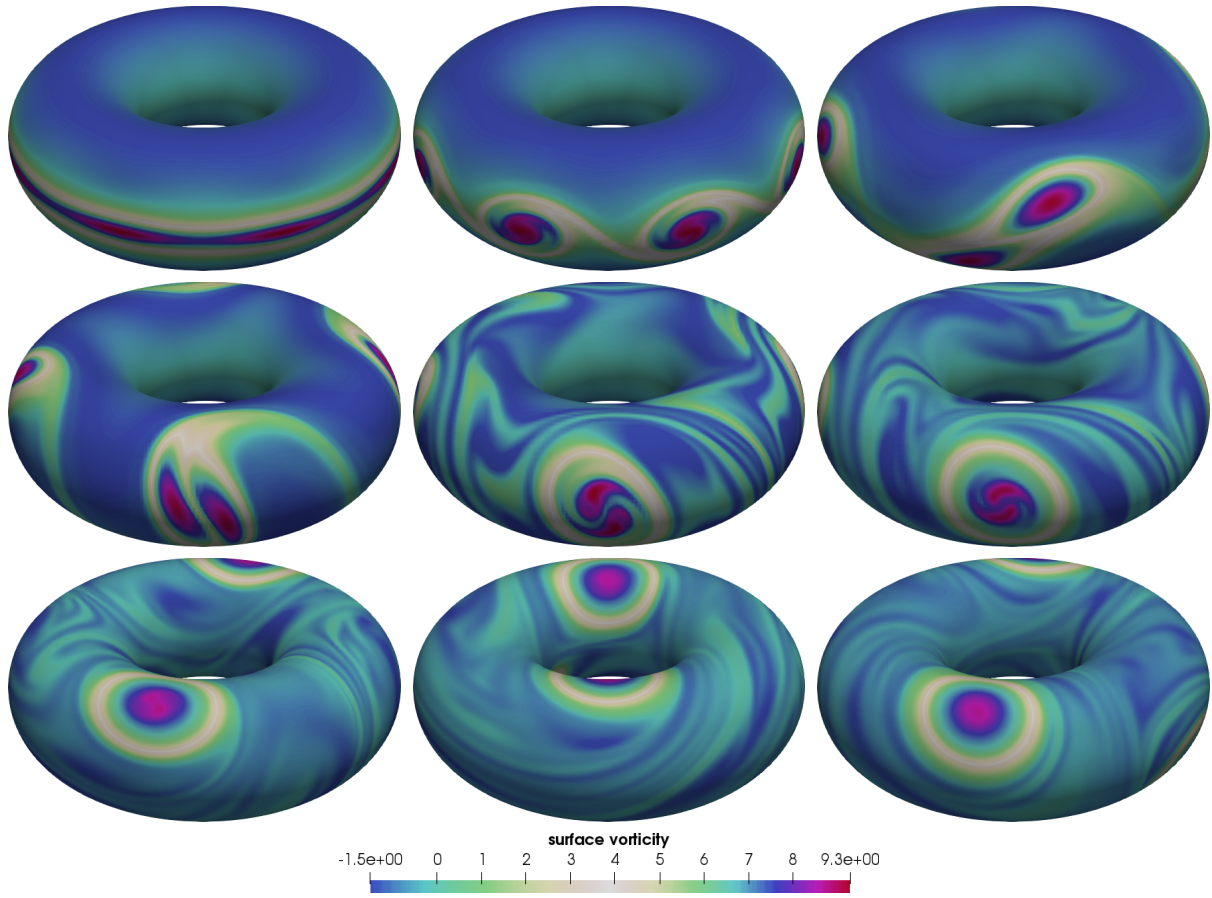


FIGURE 2 Snapshots of surface vorticity $w_h = \text{curl}_{\Gamma_h} \mathbf{u}_h$ for KH on the $R = 1, r = \frac{1}{2}$ torus for $t \in \{0, 2.3, 8.4, 9.3, 14, 18.7, 25.7, 30.4, 35\}$. Click [here](#) for the full animation.

4.2 | Solver performance

TABLE 1 Solver statistics for $\nu = \frac{1}{2} \times 10^{-4}$, varying h and $\alpha \in \{24, 48, 96\}$. Full AL preconditioner; Γ is the sphere. The total number of time steps for three mesh levels reported are 320, 640, and 1280, respectively.

# d.o.f.	T_{asmb1}	% factor steps	“fresh” LU steps			all steps		
			N_{iter}	T_{factor}	T_{insol}	N_{iter}	T_{factor}	T_{insol}
51526	3.55	3.44	9.00	1.72×10^1	0.53	33.53	0.59	2.15
203998	18.6	1.88	8.33	1.76×10^2	2.55	32.77	3.30	10.3
819862	180	0.86	7.55	1.73×10^3	12.1	29.86	14.9	49.9

In the first series of experiments we fixed the viscosity parameter equal $\frac{1}{2}10^{-4}$ and vary the mesh size. We consider three levels of mesh refinement and the number of unknowns grows by a factor of four from one level to the next one. Since $\alpha \simeq 1/\Delta t$ and $\Delta t \simeq h$, the parameter α in (4) increases two times for each refinement level. The FGMRES with full AL preconditioner was applied to solve the system of algebraic equations on each time step of (7). We use zero vector as initial guess and the drop of residual by a factor of 10^8 as the stopping criterium. Table 1 summarizes the solver averaged statistics over the time of simulation $t \in [0, 20]$. We see that the percentage of re-initializations of the preconditioner (this is when we compute new LU factors) is small and decreases for finer mesh levels. The later can be due to the growth of α and because the the diffusion term plays more significant role for smaller h . The choice of $\kappa = 5$ in (14) keeps the average number of FGMRES iterations

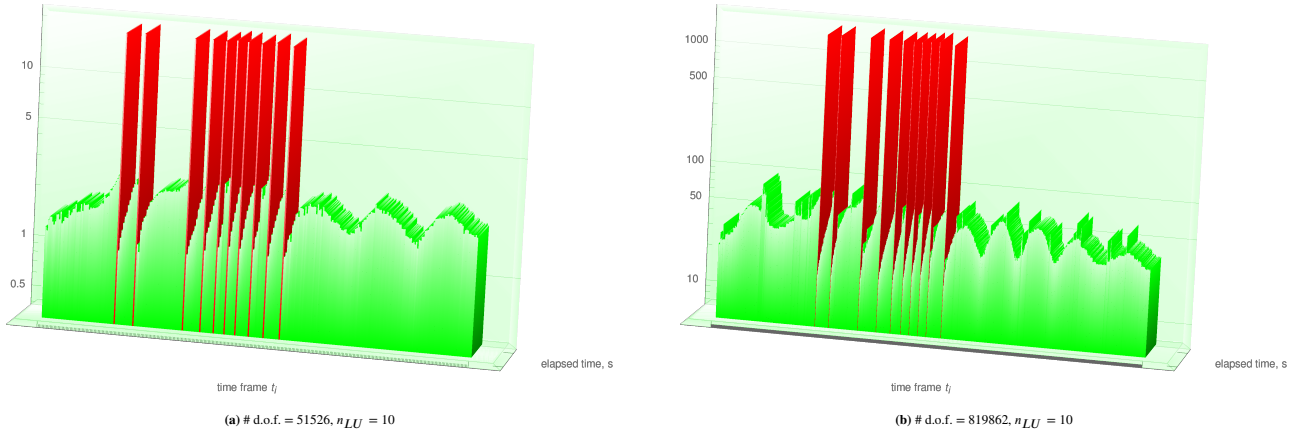


FIGURE 3 Computation time seconds (factorization and linear solve) in log-scale vs. time t_i for two different meshes. Red bars correspond to time steps for which new factors are computed; n_{LU} is a number of steps with factorizations. Full AL preconditioner; Γ is the sphere.

about 30 with very slight variation among refinement levels. To compare, the number of FGMRES iterations with ‘fresh’ LU factorization in $\hat{\mathbf{A}}$ is about 8. As expected, factorizing the matrix $\hat{\mathbf{A}}$ is by far the most computationally expensive procedure (cf. T_{factor} in “fresh LU steps” table section). However, due to the heavy and efficient recycling, overall the expense of the factorization is minor compared to the iterations cost (compare T_{factor} and T_{insol} in “all steps” table section). This allows to keep the *averaged* computation cost of the linear solver comparable and even less than the cost of matrix assembling. This balance is further visualized in Figure 3 for two mesh levels, where we see that the time steps with updated LU factors are more expensive but rare. It is interesting to note that most updates are needed for $t \in [4, 10]$, when vortices are paring. As we discussed above, the numerical integration that we use causes the assembling time to grow superlinear with respect to #d.o.f.: This is the specific of the flow problem posed on a manifold and software we use for matrix assembly.

TABLE 2 Solver statistics for fixed h (# d.o.f. = 819862) and $\alpha \simeq 100$, varying ν . Full AL preconditioner; Γ is a sphere.

ν	T_{asmbly}	% factor steps	“fresh” LU steps			all steps		
			N_{iter}	T_{factor}	T_{insol}	N_{iter}	T_{factor}	T_{insol}
$\frac{1}{2} \times 10^{-3}$	177	0.391	7.00	1.59×10^3	9.87	32.87	6.23	50.7
$\frac{1}{2} \times 10^{-4}$	180	0.859	7.55	1.73×10^3	12.1	29.86	14.9	49.9
$\frac{1}{2} \times 10^{-5}$	198	0.938	7.75	1.81×10^3	12.4	31.95	17	50.2

We repeat the simulation of the KH problem on the sphere but now for several values the viscosity parameter and the finest discretization level. All parameters of the algebraic solver are the same as above. The averaged statistics of the solver for this set of experiments are summarized in Table 2. It appears that the solver is remarkably robust with respect to the viscosity parameter. For higher Reynolds numbers we see only a slight increase of the percentage of time steps, where the preconditioner is updated by the new LU factors. Figure 4 illustrates the balance between computationally expensive but rare steps with updated preconditioner and the majority of calculations with the recycled AL preconditioner.

We now consider the surface KH flow on torus. For the given values of outer and inner radius the surface area of torus is approximately 1.57 times the surface of the unit sphere. This explains, why we get larger systems in terms of the number of degrees of freedom for the same levels of refinement in this example. This makes the problem naturally suitable for testing the recycling strategy with modified AL preconditioner. In general, the modified AL preconditioner is less robust with respect to ν and h , so its efficient use needs some tuning. Following recommendations in² we find optimal value for γ on a coarse level and then apply $1/\sqrt{2}$ -rule to scale it for finer mesh levels. This leads us to $\gamma_3 = 0.04$ for the third refinement level and $\gamma_i = 2^{\frac{3-i}{2}} \gamma_3$, $i = 4, 5, 6$, for refinement levels from 4 to 6. These are the refinement levels we use to report the solver statistics in Table 3. In

this experiment, we take the velocity field and pressure from the previous time step as the initial guess in FGMRES and relax the stopping criterium to the relative drop of residual by 10^6 , $\|\mathbf{r}_i\|_2 < 10^{-6}\|\mathbf{b}\|_2$. The number of iterations increased compared to the full AL preconditioner, since only the block upper-triangle part of the matrix \mathbf{A} is used to define $\hat{\mathbf{A}}$. We also see a slight increase of the iteration number for h getting smaller, which is also the observation in². The overall computation time is dominated by the matrix assembly because of the non-optimal numerical quadrature, as discussed above. If we take the time of assembly off the table, then the recycling strategy turns out to be very effective also with the modified AL preconditioner. The average time of factorization per one solve is negligible and each factorization is more efficient in terms of time and memory requirements since it is done for each individual velocity block. Figure 5 illustrates the balance between computationally expensive but rare steps with updated preconditioner and the majority of calculations with the recycled modified AL preconditioner.

It is out of scope for this paper to carry out a systematic comparison of the full and modified AL preconditioners. Results in this direction can be found in². For the factorize–recycle framework introduced here, our general recommendation is the following: if the storage of factors is affordable, then use the full AL preconditioner as the most robust and free of parameter tuning; otherwise switch to modified AL and adjust γ to achieve iteration numbers somewhat higher but comparable to the full AL case.

5 | CONCLUSIONS

We conclude that recycling AL preconditioner for the Oseen problem over several time steps is a highly effective strategy to reduce linear algebra costs when solving the time-dependent Navier–Stokes equations. In contrast to time-lagging of inertia terms, this approach does not compromise the numerical stability of the scheme. For many 2D flows it is feasible to compute exact factorizations of velocity sub-blocks. Within the developed framework this ensures the solver robustness with respect to the Reynolds number. The performance of the approach was illustrated for a few examples of surface flows. The efficiency evident in numerical tests were backed by eigenvalue analysis, which extends some known results to the case of FE-level stabilization. To make the method even more efficient for smaller time steps, we introduced the pressure Schur complement preconditioner, which extends the Cahouet–Chabard preconditioner for the case of non-zero (2, 2)-block \mathbf{C} . This extension can be useful in other settings with unfitted or pressure stabilized FEs.

We expect that recycled modified AL preconditioner with a threshold ILU factorization for each sub-block can be an efficient strategy for large scale 3D flow problems. We plan to explore such possibility in the future.

6 | CODE AVAILABILITY

The source code to run Kelvin–Helmholtz simulations from section 4 with building instructions and files defining input parameters was archived in⁵⁵.

7 | ACKNOWLEDGMENT

This study does not have any conflicts to disclose.

References

1. Benzi M, and Olshanskii MA. An augmented Lagrangian-based approach to the Oseen problem. *SIAM Journal on Scientific Computing*. 2006;**28**(6):2095–2113.
2. Benzi M, Olshanskii MA, and Wang Z. Modified augmented Lagrangian preconditioners for the incompressible Navier–Stokes equations. *International Journal for Numerical Methods in Fluids*. 2011;**66**(4):486–508.
3. Börm S, and Le Borne S. H -LU factorization in preconditioners for augmented Lagrangian and grad-div stabilized saddle point systems. *International journal for numerical methods in fluids*. 2012;**68**(1):83–98.

4. De Niet A, and Wubs F. Two preconditioners for saddle point problems in fluid flows. *International Journal for Numerical Methods in Fluids*. 2007;**54**(4):355–377.
5. Farrell PE, and Gazca-Orozco PA. An Augmented Lagrangian Preconditioner for Implicitly Constituted Non-Newtonian Incompressible Flow. *SIAM Journal on Scientific Computing*. 2020;**42**(6):B1329–B1349.
6. He X, Neytcheva M, and Capizzano SS. On an augmented Lagrangian-based preconditioning of Oseen type problems. *BIT Numerical Mathematics*. 2011;**51**(4):865–888.
7. He X, Vuik C, and Klaij CM. Combining the augmented Lagrangian preconditioner with the simple Schur complement approximation. *SIAM Journal on Scientific Computing*. 2018;**40**(3):A1362–A1385.
8. Heister T, and Rapin G. Efficient augmented Lagrangian-type preconditioning for the Oseen problem using Grad-Div stabilization. *International Journal for Numerical Methods in Fluids*. 2013;**71**(1):118–134.
9. Moulin J, Jolivet P, and Marquet O. Augmented Lagrangian preconditioner for large-scale hydrodynamic stability analysis. *Computer Methods in Applied Mechanics and Engineering*. 2019;**351**:718–743.
10. Olshanskii MA, and Benzi M. An augmented Lagrangian approach to linearized problems in hydrodynamic stability. *SIAM Journal on Scientific Computing*. 2008;**30**(3):1459–1473.
11. ur Rehman M, Vuik C, and Segal G. A comparison of preconditioners for incompressible Navier–Stokes solvers. *International Journal for Numerical Methods in Fluids*. 2008;**57**(12):1731–1751.
12. Farrell PE, Mitchell L, Scott LR, and Wechsung F. A Reynolds-robust preconditioner for the Reynolds-robust Scott–Vogelius discretization of the stationary incompressible Navier–Stokes equations. *arXiv preprint arXiv:200409398*. 2020;.
13. Farrell PE, Mitchell L, and Wechsung F. An Augmented Lagrangian Preconditioner for the 3D Stationary Incompressible Navier–Stokes Equations at High Reynolds Number. *SIAM Journal on Scientific Computing*. 2019;**41**(5):A3073–A3096.
14. Dahl O, and Wille S. An ILU preconditioner with coupled node fill-in for iterative solution of the mixed finite element formulation of the 2D and 3D Navier–Stokes equations. *International Journal for Numerical Methods in Fluids*. 1992;**15**(5):525–544.
15. Konshin I, Olshanskii M, and Vassilevski Y. LU factorizations and ILU preconditioning for stabilized discretizations of incompressible Navier–Stokes equations. *Numerical Linear Algebra with Applications*. 2017;**24**(3):e2085.
16. Konshin IN, Olshanskii MA, and Vassilevski YV. ILU Preconditioners for Nonsymmetric Saddle-Point Matrices with Application to the Incompressible Navier–Stokes Equations. *SIAM Journal on Scientific Computing*. 2015;**37**(5):A2171–A2197.
17. Segal A, Ur Rehman M, and Vuik C. Preconditioners for incompressible Navier–Stokes solvers. *Numerical Mathematics: Theory, Methods and Applications*. 2010;**3**(3):245–275.
18. Bonito A, Demlow A, and Licht M. A divergence-conforming finite element method for the surface Stokes equation. *SIAM Journal on Numerical Analysis*. 2020;**58**(5):2764–2798.
19. Brandner P, and Reusken A. Finite element error analysis of surface Stokes equations in stream function formulation. *ESAIM: Mathematical Modelling and Numerical Analysis*. 2020;**54**(6):2069–2097.
20. Fries TP. Higher-order surface FEM for incompressible Navier–Stokes flows on manifolds. *International Journal for Numerical Methods in Fluids*. 2018;**88**(2):55–78.
21. Gross BJ, Trask N, Kuberry P, and Atzberger PJ. Meshfree methods on manifolds for hydrodynamic flows on curved surfaces: a generalized moving least-squares (GMLS) approach. *Journal of Computational Physics*. 2020;**409**:109340.
22. Jankuhn T, Olshanskii MA, and Reusken A. Incompressible Fluid Problems on Embedded Surfaces: Modeling and Variational Formulations. *Interfaces and Free Boundaries*. 2018;**20**:353–377.

23. Jankuhn T, and Reusken A. Higher order trace finite element methods for the surface Stokes equation. Preprint arXiv:190908327. 2019;.
24. Lederer PL, Lehrenfeld C, and Schöberl J. Divergence-free tangential finite element methods for incompressible flows on surfaces. *International Journal for Numerical Methods in Engineering*. 2020;**121**(11):2503–2533.
25. Nitschke I, Reuther S, and Voigt A. Hydrodynamic interactions in polar liquid crystals on evolving surfaces. *Physical Review Fluids*. 2019;**4**(4):044002.
26. Nitschke I, Voigt A, and Wensch J. A finite element approach to incompressible two-phase flow on manifolds. *Journal of Fluid Mechanics*. 2012;**708**:418–438.
27. Olshanskii MA, Quaini A, Reusken A, and Yushutin V. A finite element method for the surface Stokes problem. *SIAM Journal on Scientific Computing*. 2018;**40**(4):A2492–A2518.
28. Olshanskii MA, Reusken A, and Zhiliakov A. Inf-sup stability of the trace P2-P1 Taylor–Hood elements for surface PDEs. *Mathematics of Computation*. 2020;.
29. Olshanskii MA, and Yushutin V. A Penalty Finite Element Method for a Fluid System Posed on Embedded Surface. *Journal of Mathematical Fluid Mechanics*. 2019;**21**(1):14.
30. Reuther S, and Voigt A. Solving the incompressible surface Navier–Stokes equation by surface finite elements. *Physics of Fluids*. 2018;**30**(1):012107.
31. Gurtin ME, and Murdoch AI. A continuum theory of elastic material surfaces. *Archive for Rational Mechanics and Analysis*. 1975;**57**(4):291–323.
32. Rangamani P, Agrawal A, Mandadapu KK, Oster G, and Steigmann DJ. Interaction between surface shape and intra-surface viscous flow on lipid membranes. *Biomechanics and modeling in mechanobiology*. 2013;p. 1–13.
33. Torres-Sánchez A, Millán D, and Arroyo M. Modelling fluid deformable surfaces with an emphasis on biological interfaces. *Journal of Fluid Mechanics*. 2019;**872**:218–271.
34. Olshanskii MA, Reusken A, and Grande J. A Finite Element method for elliptic equations on surfaces. *SIAM J Numer Anal*. 2009;**47**:3339–3358.
35. Olshanskii MA, and Reusken A. Trace Finite Element Methods for PDEs on Surfaces. In: Bordas SPA, Burman E, Larson MG, and Olshanskii MA, editors. *Geometrically Unfitted Finite Element Methods and Applications*. Cham: Springer International Publishing; 2017. p. 211–258.
36. Olshanskii MA. A low order Galerkin finite element method for the Navier–Stokes equations of steady incompressible flow: a stabilization issue and iterative methods. *Computer Methods in Applied Mechanics and Engineering*. 2002;**191**(47-48):5515–5536.
37. Olshanskii M, and Reusken A. Grad-div stabilization for Stokes equations. *Mathematics of Computation*. 2004;**73**(248):1699–1718.
38. Benzi M, Golub GH, and Liesen J. Numerical solution of saddle point problems. *Acta numerica*. 2005;**14**:1.
39. Elman H, Silvester D, and Wathen A. *Finite Elements and Fast Iterative Solvers*. Oxford: Oxford University Press; 2005.
40. Temam R. *Navier–Stokes equations, theory and numerical analysis*. Amsterdam: North-Holland; 3rd ed., 1984.
41. Girault V, and Raviart PA. *Finite Element Methods for Navier–Stokes Equations*. Berlin: Springer; 1986.
42. Burman E, Hansbo P, and Larson MG. A stabilized cut finite element method for partial differential equations on surfaces: The Laplace–Beltrami operator. *Computer Methods in Applied Mechanics and Engineering*. 2015;**285**:188–207.
43. Burman E, Hansbo P, Larson MG, and Massing A. A cut discontinuous Galerkin method for the Laplace–Beltrami operator. *IMA Journal of Numerical Analysis*. 2017;**37**(1):138–169.

44. Burman E, Hansbo P, Larson MG, and Massing A. Cut finite element methods for partial differential equations on embedded manifolds of arbitrary codimensions. *ESAIM: Mathematical Modelling and Numerical Analysis*. 2018;**52**(6):2247–2282.
45. Grande J, Lehenfeld C, and Reusken A. Analysis of a High-Order Trace Finite Element Method for PDEs on Level Set Surfaces. *SIAM Journal on Numerical Analysis*. 2018;**56**(1):228–255. Available from: <https://doi.org/10.1137/16M1102203>.
46. Olshanskii M, Lube G, Heister T, and Löwe J. Grad–div stabilization and subgrid pressure models for the incompressible Navier–Stokes equations. *Computer Methods in Applied Mechanics and Engineering*. 2009;**198**(49-52):3975–3988.
47. John V, and Kindl A. Numerical studies of finite element variational multiscale methods for turbulent flow simulations. *Computer Methods in Applied Mechanics and Engineering*. 2010;**199**(13-16):841–852.
48. Jankuhn T, Olshanskii MA, Reusken A, and Zhiliakov A. Error analysis of higher order trace finite element methods for the surface Stokes equations. *Journal of Numerical Mathematics*. 2020;.
49. Benzi M, and Wang Z. Analysis of augmented Lagrangian-based preconditioners for the steady incompressible Navier–Stokes equations. *SIAM Journal on Scientific Computing*. 2011;**33**(5):2761–2784.
50. Cahouet J, and Chabard JP. Some fast 3D finite element solvers for the generalized Stokes problem. *International Journal for Numerical Methods in Fluids*. 1988;**8**(8):869–895.
51. Schroeder PW, John V, Lederer PL, Lehenfeld C, Lube G, and Schöberl J. On reference solutions and the sensitivity of the 2D Kelvin–Helmholtz instability problem. *Computers & Mathematics with Applications*. 2019;**77**(4):1010–1028.
52. DROPS package;. <http://www.igpm.rwth-aachen.de/DROPS/>.
53. Trilinos Project Team T. The Trilinos Project Website;.
54. Lehenfeld C. High order unfitted finite element methods on level set domains using isoparametric mappings. *Computer Methods in Applied Mechanics and Engineering*. 2016;**300**:716–733.
55. DROPS: surface Navier-Stokes solver. https://github.com/56th/drops/archive/refs/heads/surfaceNSE_06/03/2021.zip; 2021.
56. Bendixson I. Sur les racines d’une équation fondamentale. *Acta Mathematica*. 1902;**25**(1):359–365.

How to cite this article: Olshanskii M.A. and A. Zhiliakov (2021), Recycling augmented Lagrangian preconditioner in an incompressible fluid solver, *Numer. Linear Algebra Appl.*,

APPENDIX

A PROOF OF (12)

Since the grad-div stabilization does not deliver the algebraic structure of the augmented Lagrangian as in^{1,2}, we cannot make use of the Sherman–Morrison–Woodbury formula or similar representations of the pressure Schur complement of the augmented system. Therefore we base our proof of (12) on a different argument. Let \mathbb{R}^m and \mathbb{R}^n be the coefficient spaces for the pressure and velocity finite element functions, respectively. For $p \in \mathbb{R}^m$ the corresponding finite element function is $p_h \in Q_h$, similar we have $\mathbf{u}_h \in \mathbf{V}_h$ for $\mathbf{u} \in \mathbb{R}^n$, etc. Further $\langle \cdot, \cdot \rangle$ denotes the Euclidian inner product and $\| \cdot \| := \langle \cdot, \cdot \rangle^{\frac{1}{2}}$.

The low bound for the real parts of the eigenvalues from (11) is given by the Bendixson theorem⁵⁶:

$$\inf_{p \in \mathbb{R}^m} \frac{\left\langle \frac{1}{2}(\mathbf{S} + \mathbf{S}^T) p, p \right\rangle}{\langle \mathbf{Q} p, p \rangle} \leq \Re(\lambda), \quad \text{with } \mathbf{Q} = (\nu + \gamma)^{-1} \mathbf{M}_p + \mathbf{C}.$$

Noting that $\langle \frac{1}{2}(\mathbf{S} + \mathbf{S}^T) \mathbf{p}, \mathbf{p} \rangle = \langle \mathbf{S} \mathbf{p}, \mathbf{p} \rangle = \langle \mathbf{B} \mathbf{u}, \mathbf{p} \rangle + \langle \mathbf{C} \mathbf{p}, \mathbf{p} \rangle$, $\mathbf{A} \mathbf{u} = \mathbf{B}^T \mathbf{p}$, we re-write the quantities on the left-hand side in the finite element notation:

$$\begin{aligned} \langle \mathbf{S} \mathbf{p}, \mathbf{p} \rangle &= b(\mathbf{u}_h, p_h) + s(p_h, p_h) \\ b(\mathbf{v}_h, p_h) &= a(\mathbf{u}_h, \mathbf{v}_h) + \gamma(\mathbf{u}_h, \mathbf{v}_h), \quad \forall \mathbf{v}_h \in \mathbf{V}_h. \end{aligned} \quad (\text{A1})$$

Letting $\mathbf{v}_h = \mathbf{u}_h$ and using the skew-symmetric form of the advection term:

$$\frac{1}{2} \int_{\Gamma} (\mathbf{v}_h^T (\nabla_{\Gamma} \mathbf{u}_h) \mathbf{w} - \mathbf{u}_h^T (\nabla_{\Gamma} \mathbf{v}_h) \mathbf{w}) \, ds, \quad (\text{A2})$$

we get

$$\langle \mathbf{S} \mathbf{p}, \mathbf{p} \rangle = a(\mathbf{u}_h, \mathbf{u}_h) + \gamma \|\operatorname{div}_{\Gamma} \mathbf{u}_h\|_{L^2(\Gamma)}^2 + s(p_h, p_h) \quad (\text{A3})$$

with \mathbf{u}_h solving the second equation in (A1) for the given p_h , i.e. $\mathbf{u} = \mathbf{A}^{-1} \mathbf{B}^T \mathbf{p}$.

Let $\|\mathbf{v}_h\|_*^2 := 2 \int_{\Gamma} |E_s(\mathbf{v}_h)|^2 \, ds + \tau \int_{\Gamma} |\mathbf{n} \cdot \mathbf{v}_h|^2 \, ds + \rho_u \int_{\Omega_h^{\Gamma}} |(\mathbf{n} \cdot \nabla) \mathbf{v}_h|^2 \, dx$. The inf-sup condition for trace \mathbf{P}_2 - P_1 elements proved in²⁸ reads:

$$c_0^2 \|p_h\|_{L^2(\Gamma)}^2 \leq \sup_{\mathbf{v}_h \in \mathbf{V}_h} \frac{b(\mathbf{v}_h, p_h)^2}{\|\mathbf{v}_h\|_*^2} + s(p_h, p_h), \quad (\text{A4})$$

with $c_0 > 0$ independent of h and position of Γ in the background mesh. The condition (A4) can be rewritten as follows: There exists $\mathbf{v}_h \in \mathbf{V}_h$ such that

$$c_0^2 \|p_h\|_{L^2(\Gamma)}^2 \leq b(\mathbf{v}_h, p_h)^2 + s(p_h, p_h), \quad \text{and } \|\mathbf{v}_h\|_* = 1.$$

We take this \mathbf{v}_h as a test function in (A1) and apply the Cauchy–Schwarz and Poincaré inequalities to arrive at

$$\begin{aligned} c_0^2 \|p_h\|_{L^2(\Gamma)}^2 &\leq [a(\mathbf{u}_h, \mathbf{v}_h) + \gamma(\mathbf{u}_h, \mathbf{v}_h)]^2 + s(p_h, p_h) \\ &\leq [a(\mathbf{u}_h, \mathbf{u}_h)^{\frac{1}{2}} a(\mathbf{v}_h, \mathbf{v}_h)^{\frac{1}{2}} + \gamma \|\operatorname{div}_{\Gamma} \mathbf{u}_h\|_{L^2(\Gamma)} \|\operatorname{div}_{\Gamma} \mathbf{v}_h\|_{L^2(\Gamma)} + \\ &\quad \|\mathbf{w}\|_{L^{\infty}(\Gamma)} \|\nabla \mathbf{u}_h\|_{L^2(\Gamma)} \|\nabla \mathbf{v}_h\|_{L^2(\Gamma)}]^2 + s(p_h, p_h) \\ &\leq [a(\mathbf{u}_h, \mathbf{u}_h)^{\frac{1}{2}} + \gamma \|\operatorname{div}_{\Gamma} \mathbf{u}_h\|_{L^2(\Gamma)} + C \|E_s(\mathbf{u}_h)\|_{L^2(\Gamma)}]^2 + s(p_h, p_h) \end{aligned}$$

where in the last inequality we used

$$a(\mathbf{v}_h, \mathbf{v}_h) \leq \|\mathbf{v}_h\|_*^2 = 1, \quad \|\operatorname{div}_{\Gamma} \mathbf{v}_h\|_{L^2(\Gamma)} \leq \|E_s(\mathbf{v}_h)\|_{L^2(\Gamma)} \leq \|\mathbf{v}_h\|_* = 1, \quad \|\mathbf{w}\|_{L^{\infty}(\Gamma)} = 1,$$

and the surface Korn inequality. Since $\|E_s(\mathbf{u}_h)\|_{L^2(\Gamma)}^2 \leq \nu^{-1} a(\mathbf{u}_h, \mathbf{u}_h)$ we obtain thanks to (A3) the estimate

$$\begin{aligned} c_0^2 \|p_h\|_{L^2(\Gamma)}^2 &\leq 3[(1 + C \nu^{-1}) a(\mathbf{u}_h, \mathbf{u}_h) + \gamma^2 \|\operatorname{div}_{\Gamma} \mathbf{u}_h\|_{L^2(\Gamma)}^2] + s(p_h, p_h) \\ &\leq 3(1 + C \nu^{-1} + \gamma) \langle \mathbf{S} \mathbf{p}, \mathbf{p} \rangle. \end{aligned}$$

Since $\|p_h\|_{L^2(\Gamma)}^2 = \langle \mathbf{M}_p \mathbf{p}, \mathbf{p} \rangle$, we get

$$\frac{c_0^2(\nu + \gamma)}{3(1 + C \nu^{-1} + \gamma)} \langle (\nu + \gamma)^{-1} \mathbf{M}_p \mathbf{p}, \mathbf{p} \rangle \leq \langle \mathbf{S} \mathbf{p}, \mathbf{p} \rangle.$$

Finally, using $\nu \leq 1$ and $\langle \mathbf{C} \mathbf{p}, \mathbf{p} \rangle \leq \langle \mathbf{S} \mathbf{p}, \mathbf{p} \rangle$ the above estimate yields

$$\frac{c(\nu + \gamma)}{\nu^{-1} + \gamma} (\langle (\nu + \gamma)^{-1} \mathbf{M}_p \mathbf{p}, \mathbf{p} \rangle + \langle \mathbf{C} \mathbf{p}, \mathbf{p} \rangle) \leq \langle \mathbf{S} \mathbf{p}, \mathbf{p} \rangle + \langle \mathbf{C} \mathbf{p}, \mathbf{p} \rangle.$$

with some c independent of h and position of Γ in the background mesh. To show the bound on $|\lambda|$, we estimate

$$|\lambda| \leq \|\mathbf{Q}^{-\frac{1}{2}} \mathbf{S} \mathbf{Q}^{-\frac{1}{2}}\| = \sup_{\mathbf{p}, \mathbf{q} \in \mathbb{R}^m} \frac{\langle \mathbf{Q}^{-\frac{1}{2}} \mathbf{S} \mathbf{Q}^{-\frac{1}{2}} \mathbf{p}, \mathbf{q} \rangle}{\|\mathbf{p}\| \|\mathbf{q}\|} = \sup_{\mathbf{p}, \mathbf{q} \in \mathbb{R}^m} \frac{\langle \mathbf{S} \mathbf{p}, \mathbf{q} \rangle}{\|\mathbf{Q}^{\frac{1}{2}} \mathbf{p}\| \|\mathbf{Q}^{\frac{1}{2}} \mathbf{q}\|}.$$

In finite element notations, we rewrite

$$\begin{aligned} \langle \mathbf{S} \mathbf{p}, \mathbf{q} \rangle &= b(\mathbf{u}_h, q_h) + s(p_h, q_h) \\ b(\mathbf{v}_h, p_h) &= a(\mathbf{u}_h, \mathbf{v}_h) + \gamma(\mathbf{u}_h, \mathbf{v}_h), \quad \forall \mathbf{v}_h \in \mathbf{V}_h. \end{aligned} \quad (\text{A5})$$

The Cauchy–Schwarz inequality yields

$$\langle \mathbf{S} \mathbf{p}, \mathbf{q} \rangle \leq \|\operatorname{div}_{\Gamma} \mathbf{u}_h\|_{L^2(\Gamma)} \|q_h\|_{L^2(\Gamma)} + s(p_h, p_h)^{\frac{1}{2}} s(q_h, q_h)^{\frac{1}{2}}$$

and

$$a(\mathbf{u}_h, \mathbf{u}_h) + \gamma \|\operatorname{div}_\Gamma \mathbf{u}_h\|_{L^2(\Gamma)}^2 = b(\mathbf{u}_h, p_h) \leq \|\operatorname{div}_\Gamma \mathbf{u}_h\|_{L^2(\Gamma)} \|p_h\|_{L^2(\Gamma)}.$$

From the second equation we get $\gamma \|\operatorname{div}_\Gamma \mathbf{u}_h\|_{L^2(\Gamma)} \leq \|p_h\|_{L^2(\Gamma)}$, and substituting this into the first equation we get

$$\langle \mathbf{S} \mathbf{p}, \mathbf{q} \rangle \leq \frac{\nu + \gamma}{\gamma} \left\| \frac{1}{\sqrt{\nu + \gamma}} p_h \right\|_{L^2(\Gamma)} \left\| \frac{1}{\sqrt{\nu + \gamma}} q_h \right\|_{L^2(\Gamma)} + s(p_h, p_h)^{\frac{1}{2}} s(q_h, q_h)^{\frac{1}{2}} \leq \frac{\nu + \gamma}{\gamma} \|\mathbf{Q}^{\frac{1}{2}} \mathbf{p}\| \|\mathbf{Q}^{\frac{1}{2}} \mathbf{q}\|.$$

This proves the desired bounds.

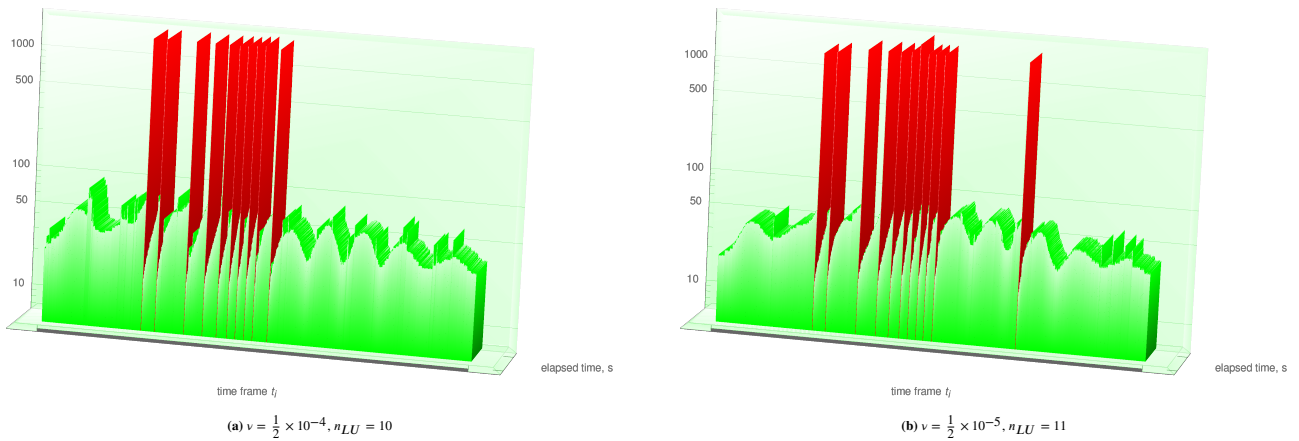


FIGURE 4 Computation time seconds (matrix assembly and linear solve) in log-scale vs. time t_i for two different viscosity parameter values. Red bars correspond to time steps for which factorization is performed; n_{LU} is a number of factorization steps. Full AL preconditioner; Γ is a sphere.

TABLE 3 Solver statistics for fixed $v = \frac{1}{2} \times 10^{-5}$, varying h and $\alpha \in \{24, 48, 96\}$. Modified AL preconditioner; Γ is a torus. The total number of time steps for three mesh levels reported are 960, 1920, and 3840, respectively.

# d.o.f.	γ	T_{asmb}	% factor steps	“fresh” LU steps			all steps		
				N_{iter}	T_{factor}	T_{insol}	N_{iter}	T_{factor}	T_{insol}
78244	0.028	7.65	6.25×10^{-1}	37.33	1.63	2.94	68.31	1.02×10^{-2}	5.02
315792	0.020	38.3	4.17×10^{-1}	42.75	18.1	16.3	75.32	7.55×10^{-2}	24.6
1279180	0.014	324	3.65×10^{-1}	64.71	181	97.6	75.51	6.61×10^{-1}	112

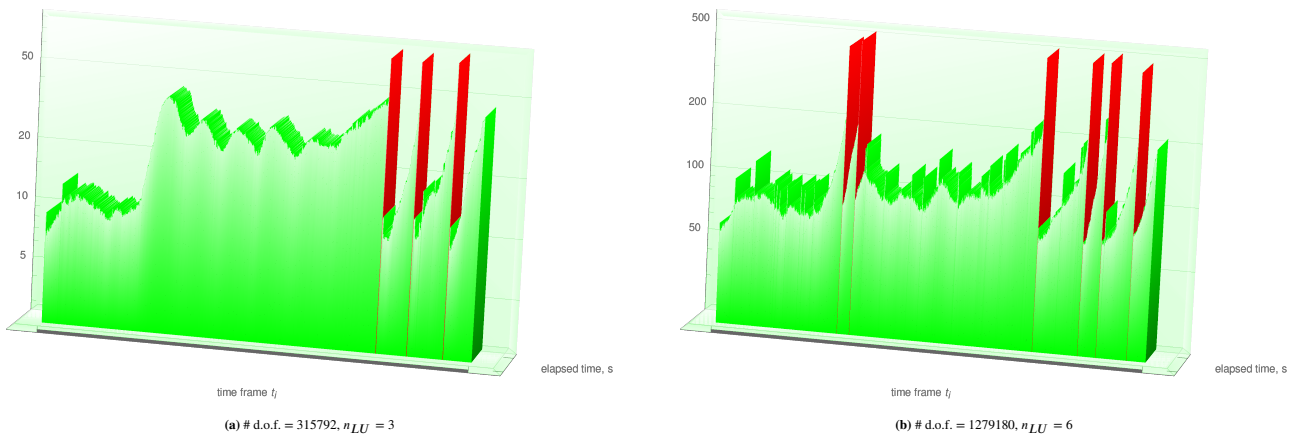


FIGURE 5 Computation time seconds (matrix assembly and linear solve) in log-scale vs. time t_i . Red bars correspond to time steps for which new factors are computed; n_{LU} is a number of steps with factorizations. Modified AL preconditioner; Γ is a torus.